NIH Public Access
Author Manuscript
Biotechnol Bioeng. Author manuscript; available in PMC 2012 June 01.

Published in final edited form as:
Biotechnol Bioeng. 2011 May ; 108(5): . doi:10.1002/bit.23024.

Optimizing the medium perfusion rate in bone tissue engineering bioreactors

Warren L Grayson[1,†], **Darja Marolt**[1], **Sarindr Bhumiratana**[1], **Mirjam Fröhlich**[1,2], **Edward Guo**[1], and **Gordana Vunjak-Novakovic**[1,*]

[1]Department of Biomedical Engineering, Columbia University, New York, NY

[2]Educell d.o.o, Ljubljana, Slovenia

Abstract

There is a critical need to increase the size of bone grafts that can be cultured *in vitro* for use in regenerative medicine. Perfusion bioreactors have been used to improve the nutrient and gas transfer capabilities and reduce the size limitations inherent to static culture, as well as to modulate cellular responses by hydrodynamic shear. Our aim was to understand the effects of medium flow velocity on cellular phenotype and the formation of bone-like tissues in three-dimensional engineered constructs. We utilized custom-designed perfusion bioreactors to culture bone constructs for five weeks using a wide range of superficial flow velocities (80, 400, 800, 1200 and 1800 μm/s), corresponding to estimated initial shear stresses ranging from 0.6 – 20 mPa. Increasing the flow velocity significantly affected cell morphology, cell-cell interactions, matrix production and composition, and the expression of osteogenic genes. Within the range studied, the flow velocities ranging from 400 to 800 μm/s yielded the best overall osteogenic responses. Using mathematical models, we determined that even at the lowest flow-velocity (80 μm/s) the oxygen provided was sufficient to maintain viability of the cells within the construct. Yet it was clear that this flow-velocity did not adequately support the development of bone-like tissue. The complexity of the cellular responses found at different flow-velocities underscores the need to use a range of evaluation parameters to determine the quality of engineered-bone.

Introduction

A major challenge in the translation of engineered viable bone grafts into large animal studies and clinical treatment of osseous defects has been the need to grow large, fully viable grafts that are several centimeters in size. The current size limitations are primarily due to the limited transport of metabolites to cells within the core regions of the graft that prevents cell survival and proliferation. Perfusion bioreactors, providing convective transfer of nutrients and oxygen, can improve homogenous development of tissues *in vitro* and have been generally proposed as a means to address this ‘size barrier’ (Grayson et al. 2008; Grayson et al. 2009; Martin et al. 2009). In previous studies, we and others have shown that the use of bioreactors with medium flow improved bone formation by human bone marrow derived mesenchymal stem cells (hMSC) as compared to static culture (Goldstein et al. 2001; Grayson et al. 2008; Marolt et al. 2006; Meinel et al. 2004a; Sikavitsas et al. 2002).

Recently, our group has validated the feasibility of cultivating large (1.5 cm × 1.5 cm × 0.5 cm), anatomically-shaped, bone grafts from hMSC in custom-designed perfusion bioreactors (Grayson et al. 2009). The spatial density of viable cells and deposition of mineralized bone

* To whom correspondence should be addressed: Dr. Gordana Vunjak-Novakovic, 622 W168th St, VC 12-234, New York NY, 10032, gv2131@columbia.edu.
† Current address: Department of Biomedical Engineering, Johns Hopkins University, Baltimore, MD

NIH-PA Author Manuscript
NIH-PA Author Manuscript
NIH-PA Author Manuscript

NIH-PA Author Manuscript

NIH-PA Author Manuscript

NIH-PA Author Manuscript

tissue matrix were markedly increased by medium perfusion through the cultured tissue constructs. We also observed strong correlations between the patterns of fluid flow in these complex tissue constructs and the patterns of bone-like tissue formation. In order to engineer thick bone constructs, it is necessary to better understand how medium perfusion rates influence the range of cellular responses, including the dynamics of osteogenic gene expression, cellular morphology and cell-cell interactions, as well as matrix formation and organization.

Whereas the primary role of perfusion has been to increase the transport rates of nutrients, metabolites and oxygen to and from the cells, interstitial flow of medium has an additional benefit of providing a hydrodynamic shear stress, a known regulatory factor of bone development and function. Prior studies have demonstrated that fluid flow stimulated rat marrow stromal cells to deposit more calcium and extracellular matrix (ECM) in 2 mm thick constructs (Bancroft et al. 2002; Sikavitsas et al. 2005). When the effects of shear stress were decoupled from the effects of nutrient transport by changing the medium viscosity at a constant flow velocity (Sikavitsas et al. 2003), the shear was shown to increase mineralized matrix deposition in a dose-dependent manner. Yet, in another study, the high shear stress associated with supra-physiological flow rates was detrimental to the viability of MC-3T3 osteoblast-like cells seeded in human trabecular bone scaffolds (Cartmell et al. 2003). In our previous work with hMSCs cultured in decellularized bovine trabecular bone scaffolds, we found that linear velocities of perfused culture medium as high as 1500 μm/s did not detrimentally affect hMSC viability, but rather resulted in improved tissue distribution throughout scaffolds (Grayson et al. 2009). For linear velocities up to 400 μm/s, estimates from simple computational models indicated that the shear stresses were still several orders lower than computed physiological values (Grayson et al. 2008; Han et al. 2004). These data suggest that the effects of flow velocity and therefore optimal conditions for *in vitro* bone formation could depend on the cell type, as well as the system used to support cell growth and bone tissue development.

In the current study, we aim to determine how medium flow velocity influences the hMSC phenotype and bone deposition in 3D constructs, to establish predictive correlations between perfusion rates and osteogenesis of hMSCs. We chose to examine a wide range of flow velocities (corresponding to the interstitial flow velocity in the range of 80 – 1800 μm/s) and evaluated cell proliferation, kinetics of osteogenic gene expression, intercellular contacts, and matrix deposition. To glean further insight, we used mathematical models to tease apart the relative contributions of oxygen delivery and biophysical stimulation as a result of the changes in flow. Our results indicate that flow velocity significantly affects bone formation patterns within cultured constructs, and provides a foundation for designing bioreactors capable of supporting the *in vitro* growth and development of bone grafts of clinically-relevant sizes.

Materials & Methods

Materials

Fetal bovine serum (FBS), Dulbecco's Modified Eagle Medium (DMEM), Penicillin–Streptomycin (Pen–Strep), Fungizone®, non-essential amino acids, trypsin/EDTA and Trizol were from Invitrogen (Carlsbad, CA). Ascorbic acid 2-phosphate, dexamethasone, sodium-β-glycerophosphate, Triton X-100 and trypsin were from Sigma-Aldrich (St. Louis, MO). Basic fibroblast growth factor (bFGF) was from Peprotech (Rocky Hill, NJ). Phosphate buffered saline (PBS), sodium carbonate, methanol and proteinase K were from Fisher Scientific (Pittsburgh, PA). All other substances were of analytical or pharmaceutical grade and obtained from Sigma-Aldrich.

NIH-PA Author Manuscript

NIH-PA Author Manuscript

NIH-PA Author Manuscript

Human Mesenchymal Stem Cells

Bone marrow-derived human mesenchymal stem cells (hMSCs) were isolated from bone marrow aspirates (Cambrex, CA) based on their attachment to tissue culture plastics as described previously (Marolt et al. 2006), expanded in high glucose DMEM supplemented with 10 % FBS, 1 ng/mL bFGF, 0.1mM non-essential amino acids, 1 % Pen–Strep and 0.2 % Fungizone (complete medium) to the 3rd passage, and used for seeding onto the scaffolds. After seeding, constructs were cultured statically in osteogenic medium specified above for 4 days to allow the cells to attach prior to placement in the perfusion bioreactors. During bioreactor cultivation, constructs were provided with osteogenic medium (high glucose DMEM supplemented with 10% FBS, 0.1mM non-essential amino acids, 1 % Pen–Strep and 0.2 % Fungizone supplemented with osteogenic supplements: 10 nM dexamethasone, 7 mM sodium-β-glycerophosphate, and 50 mg/ml ascorbic acid-2-phosphate).

Decellularized Bone Scaffolds

Bone plugs (4 mm diameter × 4 mm high) were prepared as described earlier (Grayson et al. 2008). Briefly, trabecular bone was cored from the subchondral region of carpometacarpal joints of 2-week to 4-month old cows. The plugs were washed with high velocity stream of water to remove the marrow from the pore spaces, followed by sequential washes in PBS, hypotonic buffer, detergent and enzymatic solution to remove any remaining cellular material. At the end of the process, decellularized bone plugs were rinsed repeatedly in PBS, freeze-dried and cut to 4 mm length to obtain scaffolds for cell cultivation. The dry weights and exact length of the plugs were measured and used to calculate the scaffold density and porosity. Scaffolds were sterilized in 70% ethanol for at least one hour and incubated in culture medium overnight prior to cell seeding.

Construct Assembly and Perfusion Bioreactor Culture

Cells of the 3rd passage were resuspended at a seeding density of 30×10^6 cells/ml. A 40 μL aliquot of the cell suspension was pipetted to the top of blot-dried scaffolds and allowed to percolate through. Every 15 minutes, for 1 hr, the scaffolds were rotated 180° to facilitate uniform cell-distribution. Each time, 5 μL of medium was added to prevent the cells from drying out. The resulting constructs were then placed in six well plates (1 scaffold per well) and 6 ml of medium added. The seeding efficiency was determined by evaluating the DNA content of scaffold immediately after the seeding process and comparing these to DNA samples of the total cell number seeded into scaffolds. After 4 days, constructs (6 per group) were transferred to perfusion bioreactors (time = 0) and cultured for up to 5 weeks. Each bioreactor enabled simultaneous cultivation and uniform perfusion of six scaffolds. Culture medium is pumped through an inlet port, and evenly distributed through the six channels. The resistance to flow through the channels is higher than that encountered as medium flows through the scaffolds, to reduce the flow dependence on the scaffold permeability. Low Reynolds numbers are maintained through the system so that laminar flow profiles can be approximated. A multi-channel peristaltic pump is used to maintain re-circulating flow. The flow rate is determined by the cross-sectional area of the tube as the length of the column of fluid being pumped and the rate of pumping remains constant among groups.

Bioreactor systems were set-up as described in our previous work (Frohlich et al. 2010; Grayson et al. 2008) and the superficial velocities of 80, 400, 800, 1200 or 1800 μm/s were set by using tubing of different diameters for each bioreactor in the channels of the same multi-channel peristaltic pump (Ismatec). Culture medium in the bioreactor was constantly re-circulated, and maintained in equilibrium with the atmosphere in the incubator. These conditions established the oxygen concentration of 20% at the inlet of each construct (Fig. 1). During culture, 50% of the medium volume was exchanged twice weekly with fresh medium, and medium samples were taken for biochemical assays at each medium change.

NIH-PA Author Manuscript

NIH-PA Author Manuscript

NIH-PA Author Manuscript

Constructs were harvested after one day, one week and five weeks of perfusion culture and distributed for assessments as follows: four constructs from each group were cut into halves, weighed and used for the evaluation of the DNA content and RNA levels of bone matrix proteins. The remaining two constructs from each group were fixed, imaged by micro-computerized tomography (μCT), and sectioned for histological evaluation.

Live-Dead assay

Constructs were cut in half and incubated with calcein AM (indicating live cells) and ethidium homodimer-1 (indicating dead cells) according to manufacturer's protocol (LIVE/DEAD (R) Viability/Cytotoxicity Kit, Molecular Probes) and then observed and imaged on a confocal microscope. Optical slices were taken from the surface at 10 μm intervals, up to the depth of 160 μm and then presented as a vertical projection.

DNA assay

Tissue constructs were washed in PBS and then placed in 1 ml of digestion buffer (10 mM Tris, 1mM EDTA and 0.1% Triton X-100) with 0.1mg/mL proteinase K in micro-centrifuge tubes. Constructs were incubated over night at 60 °C. The supernatants were collected and diluted 10 times to bring into the linear range of the Picogreen assay. A standard curve was prepared from a solution of salmon testes DNA obtained from Molecular Probes. Picogreen dye (Molecular Probes, OR) was added to the samples in duplicate in 96-well plates (100 μL dye into each100 μL sample) and read in a fluorescent plate reader (excitation 485 nm: emission 530 nm).

Gene expression

RNA was isolated from the tissue constructs and quantified as described previously (Meinel et al. 2004b). Briefly, the constructs were disintegrated in 1ml of Trizol using steel balls and the Mini-Beadbeater (Biospec, Bartlesville, OK). Suspensions were centrifuged at 12,000 **g** for 10 minutes at 4 °C to remove tissue debris and extracted with chloroform. The aqueous phase was collected, mixed with equal volume of 70% ethanol and applied to an RNeasy mini spin column (Qiagen, Valencia, CA). RNA was then purified according to the manufacturer's instructions. Approximately 1 μg of RNA was reversely transcribed with random hexameres (SuperScript III First-Strand Synthesis System, Invitrogen). Osteopontin, bone sialoprotein (BSP), osteocalcin and the housekeeping gene glyceraldehyde-3-phosphate-dehydrogenase (GAPDH) expression were quantified using the ABI Prism 7900 real time system (Applied Biosystems, Foster City, CA). Primer sequences for the human osteocalcin gene were: 5′-GAAGCCCAGCGGTGCA -3′ (forward primer), 5′-CACTACCTCGCTGCCCTCC -3′ (reverse primer), 5′-TGGACACAAAGGCTGCACCTTTGCT -3′ (probe, labeled with FAM and TAMRA) (Martin et al. 2001). Primers and probes for osteopontin (Assay on Demand # Hs00167093_ml), BSP (Assay on Demand # Hs00173720_ml) and GAPDH (Endogenous Control # 4310884E) were purchased from Applied Biosystems. The expression data were normalized to GAPDH and presented as average values for each group/time point.

Osteopontin ELISA

Aliquots of spent medium from the bioreactors were collected at each medium change and stored at -80°C. The concentration of osteopontin was measured with a human osteopontin ELISA kit using a standard curve developed according to the manufacturer's instructions (R&D Systems, Minneapolis, MN).

NIH-PA Author Manuscript

NIH-PA Author Manuscript

NIH-PA Author Manuscript

Histology & Immunohistochemistry

Constructs were washed in PBS and fixed in 10% formalin for 1 – 2 days. Samples were then decalcified for 2 days with Immunocal solution, dehydrated with graded ethanol washes, embedded in paraffin, sectioned to 5 μm and mounted on glass slides (all four groups were on the same slide with 2 sections per experimental group). Samples were stained using H&E, trichrome, and immunohistochemistry stainings for collagen I, bone sialoprotein (BSP), osteopontin and osteocalcin. For immunostains, the sections were deparaffinized with Citrisolv and rehydrated with a graded series of ethanol washes. For collagen, the sections were incubated in 0.01% trypsin, blocked with normal serum, stained with primary antibodies (collagen 1: mouse monoclonal anti-collagen I from Abcam (ab6308); BSP: rabbit polyclonal anti-bone sialoprotein II from Chemicon (AB1854). For osteopontin, rabbit polyclonal anti-osteopontin from Chemicon (AB1870) was used, followed by the secondary antibody and development with a biotin/avidin system. The serum, secondary antibody and developing reagents were obtained from Vector Laboratories and included in the Vector Elite ABC kit (universal) (PK6200) and DAB/Ni Substrate (SK-4100). Negative controls were performed by omitting the primary antibody incubation step.

Semi-quantitative analysis of the amounts and distributions of bone proteins was conducted using ImageJ. Each image was converted to an RGB Stack and the Green stack was used. Thresholding was performed using a value of 170 for the OCN files (from the average intensity of the negatively stained images). Grids were generated and 5 grids were chosen arbitrarily from each slide (avoiding the areas of original bone matrix). The fractional area covered and intensity of stains were measured fort each section.

Micro Computerized Tomography (μCT)

μCT was performed using a modification of a previously developed protocol (Liu et al. 2006). After fixation with glutaraldehyde, the samples were aligned along their axial direction and stabilized with wet gauze in a 15 mL centrifuge tube that was clamped in the specimen holder of a vivaCT 40 system (SCANCO Medical AG, Basserdorf, Switzerland). The 4 mm length of the scaffold was scanned at 21 μm isotropic resolution. The total bone volume (BV), which consists of the bone matrix in the scaffold and the new mineralized bone, was obtained from the application of a global thresholding technique so that only the mineralized tissue is detected. The bone volume fraction (BVF) was calculated by dividing the BV by the volume of the sample. Spatial resolution of this full voxel model was considered sufficient for evaluating the micro-architecture of the samples.

Mathematical Model for Hydrodynamic Shear Stress—To determine shear stress imparted to cells at the beginning of culture, the geometry of the bone scaffolds was modeled as a bundle of hollow cylinders arranged in parallel (Grayson et al. 2008). The internal diameters of the cylinders were varied while maintaining the overall void volume at 70 % to determine the correlation of the wall shear stresses with pore size for a given linear flow-velocity. The relationship for shear-stress was given by:

$$\tau_w = \frac{8 \cdot \mu \cdot u}{d_c} \quad (1)$$

Where τ_w is the wall shear stress, μ is the viscosity of the medium, u is the velocity and d_c is the diameter of the channels.

NIH-PA Author Manuscript

NIH-PA Author Manuscript

NIH-PA Author Manuscript

Mathematical Model for Oxygen Distribution—Oxygen concentrations inside the scaffolds were simulated in COMSOL Multiphysics program. The computation and constants were based on a previously reported approach (Flaibani et al. 2010) while accounting for differences in geometry and applying the pseudo steady-state condition. The bone construct was modeled as a volume consisting of 45 parallel channels, each 500 μm in diameter and 4 mm long, aligned axially and totaling a void volume of 70%. By assuming equal distribution of fluid flow between the channels, that is consistent with the histological evidence of uniform tissue formation, the model could be reduced to the single channel model.

The governing equations were derived with axial symmetry for cylindrical geometry, assuming the cells grow from the channel walls into the channel lumens. Two regions were modeled for O_2 transport: bulk medium phase and the cell-layer region. The transport through the bulk medium phase was described by the Navier-Stokes and convection-diffusion modules, and the transport through the cell layer was modeled by using only the convection-diffusion module. The governing Navier-Stokes equations for incompressible flow were given by:

$$\rho\frac{\partial u}{\partial t} - \nabla \cdot \eta\left(\nabla u + (\nabla u)^T\right) + \rho(u \cdot \nabla)u + \nabla p = F \quad (2)$$

$$\nabla \cdot u = 0 \quad (3)$$

where ρ is the medium density (1000 kg/m^3), η is the dynamic viscosity (7.7 × 10^{-4} Pa•s), u is the velocity vector, p is the pressure (constant), and F is the gravity. The velocities were set to the linear flow velocities of the culture medium (80, 400, 800, 1200 and 1800 μm/s) and bone channel geometries. The governing convection-diffusion equation is:

$$\frac{\partial c}{\partial t} = D\nabla^2 c - u \cdot \nabla c + R$$

where c is O_2 concentration (mol/m^3), D is the diffusion co-efficient (3.29 × 10^{-9} m^2/s in the medium region (Chow et al. 2001; Flaibani et al. 2010) and 2.0 × 10^{-9} m^2/s in the cell layer (Flaibani et al. 2010; Macpherson et al. 1997), and R is the O_2 consumption rate which followed the Michaelis-Mentin kinetics, an assumption based on our previous studies and the related published work (Coletti et al. 2006; Flaibani et al. 2010; Obradovic et al. 2000; Radisic et al. 2005; Radisic et al. 2006):

$$R = -\frac{1}{\nu_{cell}}\frac{Q_m c}{C_m + c} \quad (4)$$

where ν_{cell} is the cell volume, Q_m is the maximal oxygen consumption rate (1.86 × 10^{-18} mol/cell/s (Flaibani et al. 2010; Obradovic et al. 2000) and C_m is the oxygen concentration at half-maximal oxygen consumption (6.0 × 10^{-3} mol/m^3) (Flaibani et al. 2010; Obradovic et al. 2000).

The dissolved oxygen concentration at the inlet to the construct was assumed to be in equilibrium with air (C_O = 2.1 × 10^{-1} mol/m^3), and medium was perfused from the bottom of the constructs upwards through the channels. Therefore, the O_2 concentrations at the bottom of the channels were kept constant at C_O. The model was based on the cell number at

NIH-PA Author Manuscript

NIH-PA Author Manuscript

NIH-PA Author Manuscript

the end of the cultivation period (obtained from DNA data), and it was solved to determine whether oxygen became limiting in the system. The cell layer thickness that correlated with the experimental cell number was 7 μm, using the previously reported single cell volume of 1.44×10^{-15} m^3/cell (Flaibani et al. 2010). Four additional cell layer thicknesses (50, 100, 150 and 200 μm) were analyzed, while maintaining the cell number constant and varying the cell volume, to determine the O_2 concentration profile and the minimum O_2 concentration in the cell layer.

Statistical Analysis

Comparisons between the groups at the same time point or within a single group at three different time points were carried out by one-way ANOVA followed by Tukey's post-hoc analysis using STATISTICA software. $P < 0.05$ was considered as statistically significant.

Results

Cell proliferation

The cell seeding efficiency into the porous scaffolds was 92.4 ± 7.2 % (Supplementary Fig. 1). After four days of static cultivation, 73.5 ± 26.3 % of these cells were still in the scaffolds. This was an average of $7.7 \pm 2.0 \times 10^5$ cells per construct at the beginning of bioreactor cultivation, corresponding to a spatial cell density of $15.4 \pm 4.0 \times 10^6$ cells/cm^3. Even at such high seeding densities, the cell numbers roughly doubled during the first week of culture irrespective of the medium flow velocity (Fig. 2). The cells remained viable (as verified by live-dead assay; data not shown), with no further net increase in cell numbers beyond the first week, for up to the five weeks of bioreactor cultivation. The final cell number was $1.4 \pm 0.1 \times 10^6$ cells per construct at the end of the cultivation period (average for all experimental groups).

Bone matrix formation and cellular morphology/connectivity

H&E stains demonstrated a clear effect of flow velocity on the distribution of cells and matrix throughout the constructs (Fig. 3 **top row**). The extracellular matrix (ECM) deposition within the constructs increased gradually in uniformity and density with increasing flow velocities from 80 to 1800 μm/s. In the groups with the flow velocities of 400 - 1800 μm/s, the matrix formation and cell distribution at the edges (Fig. 3, **second row**) appeared similar to those at the centers of the constructs (Fig. 3, **third row**).

The high magnification images of histological sections also demonstrated that cells exhibit increasingly elongated morphologies at higher flow velocities. We examined the connexin-43 expression in cells within constructs and found that the characteristic punctate expression of this protein was evident only in constructs grown at flow velocities of 400 and 800 μm/s (Fig. 3, **bottom row**, white arrows). Immunohistochemical analysis was used to evaluate the presence of bone-specific proteins in the constructs. As it was with matrix production, it was found that the amount of proteins (osteopontin, osteocalcin and collagen I) in the matrices also increased with the higher flow velocities (Fig. 4, **top three rows**). μCT data indicated the maintenance of a trabecular structure in all groups (Fig. 4, **bottom row**). The variability in the mineral volume of decellularized bone scaffolds prior to cultivation of cells prevented statistically accurate comparisons of mineral volumes among groups after cultivation.

Quantitative expression of bone-specific markers—RT-PCR assays were used to determine the relative expression of osteopontin, osteocalcin and bone-sialoprotein in constructs at 1 day, 1 week and 5 weeks of bioreactor cultivation. Osteopontin expression increased significantly during the first week in all groups. At week 5, the expression

NIH-PA Author Manuscript

NIH-PA Author Manuscript

NIH-PA Author Manuscript

increased further for the 80 μm/s group, was constant for the 400 μm/s group and decreased for the other three groups (800 – 1800 μm/s) so that the expression at week 5 was comparable to the day 1 expression in these groups (Fig. 5, **top graph**). The trends in osteocalcin expression were similar among all five groups: the OCN expression was identical at day 1 and week 1 in all groups but then showed a statistical increase at week 5 (Fig. 5, **middle graph**). Like OCN, the trend in BSP expression was similar among the five groups: there was minimal expression at day 1, followed by a considerable increase in expression at week 1 and a statistically significant increase at week 5 in all groups (Fig. 5, **bottom graph**). Interestingly, a trend of decreasing OPN, OCN and BSP gene expression was observed with increasing flow velocities at all time points evaluated, and in particular after 5 weeks of culture.

The OPN protein content in the medium was evaluated at each medium change using the ELISA assay. It was observed that OPN levels increased significantly over time in the groups cultured with 80 and 400 μm/s flow velocities, while there was very little change in concentration for the 1200 and 1800 μm/s groups (Fig. 6). Interestingly, at week 5, the OPN content in the media of different groups closely correlated with the pattern of gene expression at the same time point.

Shear-stress distribution—Using a model developed in our previous studies to estimate the levels of shear stress within the freshly seeded constructs as a function of the flow-velocities (Grayson et al. 2008), we found that at the 80 μm/s flow-velocity the shear stress was in the constructs was an average 0.6 mPa. The values of shear stress increased with increasing flow-velocities to 2 - 20 mPa for flows ranging from 400 – 1800 μm/s respectively (Fig. 7).

Oxygen distribution—The oxygen distribution was based on the final cell numbers in the constructs at the end of cultivation, since this can be considered the most transport-limiting case. In this model, the cell thickness at the walls was as low as 7 μm if uniform distribution of cells among all the channels was assumed. Under these conditions, even at the lowest flow velocity (80 μm/s) oxygen was not limiting in the central regions of the scaffold (Fig. 7). Since the cell layer also consisted of extracellular matrix (ECM), the model was extended to show an increasing cell layer thickness while maintaining the cell number by altering the cell volume parameter, ν_{cell}, to represent the cell and matrix volumes together. This resulted in a steeper gradient along the channels to a minimum value of 0.205 mol/m^3 in the center of the channels (Fig. 7). Hence, based on the analysis of the most limiting case (lowest flow and highest cell volume) for our system, the amount of oxygen available to the cells was shown to be sufficient at all higher flow-velocities (400 – 1800 μm/s).

Discussion

The demand for viable bone substitutes has motivated advanced tissue engineering approaches for growing clinically sized bone grafts. For over 15 years, the significance of interstitial flow of medium to engineered bone tissues has been recognized (Hillsley and Frangos 1994) and the use of perfusion bioreactors has been integral for enabling the formation of large grafts as well as providing insight into the underlying mechanisms of bone formation. Yet, our understanding of the combined effects of medium perfusion rates on stem cell growth, differentiation and tissue formation within 3D constructs is limited. Several prior studies have compared the effects of dynamic versus static systems using various types of bioreactor systems (Bjerre et al. 2008; Frohlich et al. 2010; Glowacki et al. 1998; Goldstein et al. 2001; Stiehler et al. 2009), while others have investigated dose-dependent effects of flow (Bancroft et al. 2002; Cartmell et al. 2003; Grayson et al. 2008).

NIH-PA Author Manuscript

NIH-PA Author Manuscript

NIH-PA Author Manuscript

The present study utilized hMSCs cultured on bone scaffolds in a bioreactor with medium perfusion (interstitial flow through the cultured construct), and was designed to investigate the effects of perfusion velocity on the development of engineered human bone. The eventual goal is to facilitate optimization of flow conditions for growing large bone grafts. However, the cells are known to exhibit substrate-specific interactions that influence their spreading and responses to external stimuli (Salvi et al.). Therefore, the reported findings are directly relevant only to the cultivation of hMSCs on decellularized bone scaffolds.

Multiple engineering and biological parameters were measured and analyzed to gain a more comprehensive understanding of *in vitro* bone-like tissue development and the cultivation conditions required to generate functional tissues. In previous studies, we showed that static culture of hMSCs on trabecular bone scaffolds yielded constructs with empty centers and that flow is required for tissue development in the scaffold interiors (Grayson et al, 2008, Grayson et al, 2009). In this study, we aimed to understand what levels of flow induce the most favorable response, and the different flow groups were used as each other's control instead of comparing to static (no flow) culture conditions. Notably, the cells were uniformly distributed throughout the scaffold immediately upon seeding. However, the subsequent deposition and assembly of extracellular matrix depended on the conditions of convective transfer of nutrients and oxygen throughout the construct. The density and homogeneity of the engineered tissue depended on the perfusion velocity, which in turn determined the rate of mass transport.

Our study shows that there is no single flow velocity that yielded the best results for every measured outcome. Instead, there appeared to be an optimal range of flow velocities of 400 - 800 μm/s that resulted in the highest matrix deposition. In fact, with respect to specific trends, it was found that there were four categories of the effects of medium perfusion rate: (i) No variability between groups (for DNA), (ii) Increase with an increase in flow velocity (for cell elongation, tissue uniformity), (iii) Optimum value of medium perfusion velocity (for matrix density and connexin-43 expression), and (iv) Decrease with an increase in medium perfusion velocity (gene expression). The matrix distribution (shown by the H&E stains in Figure 3) clearly shows the 800 μm/s group as the best and the 80 μm/s group as the worst in that respect. The RT-PCR and ELISA data showed lowest relative expression of bone-specific genes in the 1200 and 1800 μm/s groups. The connexin-43 expression was evident only in the 400 and 800 μm/s groups. Based on these individual assays, we concluded that the best combination of factors was observed in the 400 and 800 μm/s groups, suggesting that an optimal flow-velocity may lie between those two values.

It is significant that even though a relatively high seeding density was used, the cell numbers doubled over the first week of culture, resulting in cell densities as high as 1.4×10^6 cells per scaffold (corresponding to $2.8 \pm 0.3 \times 10^7$ cells/cm^3). After the first week, cell numbers stabilized at this value, and cells continued to synthesize and deposit mineralized ECM. The growth kinetics data in the present study indicated that the final cell number was achieved fairly quickly – after one week – and then stabilized for the duration of culture. The hMSCs appeared more spread and elongated with increasing flow rates, indicating a definite morphological response to hydrodynamic stimulation (Fig. 3). The cells and matrix showed distinct alignment in microscopic regions of the graft, presumably in the direction of medium streamlines (Maes et al. 2009). This effect of flow suggests that future bioreactor designs may consider methods for inducing cell and tissue alignment throughout the entire matrix as this would be more consistent with native bone architecture and may enhance integration.

Cells cultured at the flow velocities of 400 – 800 μm/s exhibited the highest expression of connexin 43. Connexin 43 is expressed at the onset of mesenchymal condensation (Zhang et

NIH-PA Author Manuscript

NIH-PA Author Manuscript

NIH-PA Author Manuscript

al. 2002), in undifferentiated mesenchymal stem cells (Grayson et al. 2007), in mature osteoblasts and osteocytes (Stains and Civitelli 2005; Zhang et al. 1998; Zhang et al. 2002), and is a crucial protein regulating the bone (and cartilage) formation. Transformed cells over-expressing connexin 43 exhibited increased magnitude and spatial distribution of gap junctions and osteogenic differentiation markers throughout the construct volume, and transplantation of these cells resulted in an increased volume fraction and spatial uniformity of bone *in vivo* (Rossello et al. 2009). In this study, we found the expression of connexin 43 only at 400 and 800 μm/s flow velocities, indicating that these conditions favor cell connectivity.

Osteogenic differentiation of hMSCs was confirmed via the upregulation of bone specific genes. In particular, OCN and BSP, which are expressed at the latter stages of osteogenic differentiation, were significantly upregulated at the end of cultivation in all groups consistent with earlier reports (Meinel et al. 2004b). The expression of all three genes - OPN, OCN and BSP - at week 5 decreased with an increase in flow velocity (Fig. 5). Prior studies have shown that the expression of these markers increased in the presence of medium flow relative to static cultures (Yu et al. 2004) and other studies have suggested that higher flows and/or shear stresses should induce greater bone differentiation and tissue formation (Bancroft et al. 2002; Sikavitsas et al. 2003). However, that conclusion was based primarily on calcium secretion and matrix formation. In their studies, a positive correlation between flow velocity and osteopontin secretion was detected only during the first week of cultivation, and the trend was reversed by Day 16 of culture (Bancroft et al. 2002). Clearly, corroborating data is needed to draw conclusions about the flow dependence of osteogenic gene expression.

Therefore, to further understand the trends in the OCN, OSP and BSP gene expression, we tried to correlate the gene expression data with histological observations. Histology data indicated that the amount of OPN, OCN and collagen I in the matrix increased with perfusion rates up to 800 μm/s and then either decreased slightly (OPN) or remained constant (OCN, collagen I and BSP (not shown). One possible explanation is that the increased OPN and OCN being produced by the cells at the lower flow velocities are not being retained in the ECM due to the decreased matrix content in the constructs in these groups. This explanation is consistent with the results of the ELISA assay, which demonstrated that the amount of OPN released into the medium increased exponentially over time in the 80 and 400 μm/s groups and remained low throughout the five-week cultivation period for the 800, 1200 and 1800 μm/s groups. Taken together, these data show again that bone-like tissue formation is a rather complex process, both *in vivo* and *in vitro*, and that many factors must be considered in parallel to enable useful conclusions to be drawn regarding the selection of cultivation conditions for stem cell growth, differentiation and tissue formation. It should also be emphasized that this system deals specifically with hMSCs in trabecular bone scaffolds. It is possible that the cellular responses would be quite different if a different scaffold type were used.

An interesting question is one related to the relative contributions of shear-stress and oxygen supply to the cells on tissue development. Recent studies in other laboratories employed finite element analysis (FEA) to evaluate the stresses to which cells are exposed either in 3D constructs on in cell monolayers (Porter et al. 2005; Voronov et al.; Voronov et al.). These approaches were most useful in direct studies of cell biomechanics, and the situations where the biomaterial scaffold can be replicated with great fidelity. In our studies, native trabecular bone was used as a substrate for regenerating bone grafts, and the FEA analysis would not necessarily provide information for generalizing the process. Instead, the analysis would have to be repeated for each individual scaffold. In addition, the internal geometry of tissue constructs changes with time Based on this rationale, we developed a simple model of shear

NIH-PA Author Manuscript

NIH-PA Author Manuscript

NIH-PA Author Manuscript

stress that assumed the constructs could be modeled as a bundle of parallel, hollow cylinders, as in our previous study (Grayson et al. 2008). Despite the simplicity of this model, the results show very good agreement with the finite modeling approaches models that account for the complex internal geometry of the tissue constructs (Cioffi et al. 2006; Maes et al. 2009; Porter et al. 2005).

At the highest flow rates utilized in the study (>1000 μm/s), the wall shear stress remained at least one order of magnitude lower (20 mPa) than that calculated for native bone (1 – 3 Pa) (Zeng et al. 1994). However, as this was estimated at the beginning of the cultivation period, the values in engineered bone constructs are likely to be considerably higher at the end of the cultivation period when cells and matrix fill the pore spaces. It is not inconceivable that under these end-stage conditions cells start to experience shear stresses similar to native values. Even so, the effects may be intrinsically different from the physiological situation given that the shear remains constant for extended periods rather than oscillating, as occurs within the interstitial spaces of native bone (Jacobs et al. 1998; You et al. 2001). This suggests a need for experiments in which the flow rate would be varied to more closely mimic physiological conditions.

Oxygen was also modeled using the same simplified geometric model of parallel channels of uniform diameter used for modeling the hydrodynamic shear. It is noted that the model is limited by assuming dense cellular packing along the walls of a cylinder and growing into the channel space, as opposed to uniformly distributed cells organized within an extracellular matrix. A range of oxygen consumptions based on previously reported values were used in the model for the most limiting case of oxygen demand (highest cell number). According to the model predictions, oxygen did not becoming limiting even at the lowest flow velocity. While there was a gradient in oxygen levels in the axial direction, the lowest levels (~ 0.205 mol/m^3) were still significantly higher than threshold values calculated from previous studies (5.26×10^{-2} mol/m^3) (Flaibani et al. 2010). The oxygen analysis seems to suggest that the major influence of perfusion in our systems was the biophysical stimulation rather than oxygen supply to the cells.

Conclusions

Engineering functional bone constructs that would have clinical utility for repairing large bone defects is rather challenging goal, due to our still incomplete understanding of the individual and combined effects of factors that determine bone development and function *in vitro*. In this study, we examined the effects of a wide range of medium flow rates (80 – 1800 μm/s) on the formation of engineered bone constructs by human mesenchymal stem cells cultured on bone scaffolds. Taken together, the experimental data and mathematical modeling show that the linear velocity of medium perfusion in the range of 400 - 800 μm/s was optimal in our system based on histological analyses, connexin expression and protein contents. As mathematical modeling suggests that oxygen does not limit cell viability in this range of flow rates, the major differences among the groups appear to be mediated by the biophysical effects of medium flow.

Supplementary Material

Refer to Web version on PubMed Central for supplementary material.

Acknowledgments

We gratefully acknowledge funding support of this work by the NIH (DE161525 and EB02520 to GVN) and NYSCF (Stanley and Fiona Druckenmiller Fellowship to DM)

NIH-PA Author Manuscript

NIH-PA Author Manuscript

NIH-PA Author Manuscript

References

Bancroft GN, Sikavitsast VI, van den Dolder J, Sheffield TL, Ambrose CG, Jansen JA, Mikos AG. Fluid flow increases mineralized matrix deposition in 3D perfusion culture of marrow stromal osteloblasts in a dose-dependent manner. Proceedings of the National Academy of Sciences of the United States of America. 2002; 99(20):12600–12605. [PubMed: 12242339]

Bjerre L, Bunger CE, Kassem M, Mygind T. Flow perfusion culture of human mesenchymal stem cells on silicate-substituted tricalcium phosphate scaffolds. Biomaterials. 2008; 29(17):2616–2627. [PubMed: 18374976]

Cartmell SH, Porter BD, Garcia AJ, Guldberg RE. Effects of medium perfusion rate on cell-seeded three-dimensional bone constructs in vitro. Tissue Engineering. 2003; 9(6):1197–1203. [PubMed: 14670107]

Chow DC, Wenning LA, Miller WM, Papoutsakis ET. Modeling pO(2) distributions in the bone marrow hematopoietic compartment. I. Krogh's model. Biophysical Journal. 2001; 81(2):675–684. [PubMed: 11463616]

Cioffi M, Boschetti F, Raimondi MT, Dubini G. Modeling evaluation of the fluid-dynamic microenvironment in tissue-engineered constructs: A micro-CT based model. Biotechnology and Bioengineering. 2006; 93(3):500–510. [PubMed: 16224789]

Coletti F, Macchietto S, Elvassore N. Mathematical modeling of three-dimensional cell cultures in perfusion bioreactors. Industrial & Engineering Chemistry Research. 2006; 45(24):8158–8169.

Flaibani M, Magrofuoco E, Elvassore N. Computational Modeling of Cell Growth Heterogeneity in a Perfused 3D Scaffold. Industrial & Engineering Chemistry Research. 2010; 49(2):859–869.

Frohlich M, Grayson WL, Marolt D, Gimble J, Kregar-Velikonja N, Vunjak-Novakovic G. Bone Grafts Engineered from Adipose-Derived Stem Cells in Perfusion Bioreactor Culture. Tissue Eng A. 2010; 16(1):179–189.

Glowacki J, Mizuno S, Greenberger JS. Perfusion enhances functions of bone marrow stromal cells in three-dimensional culture. Cell Transplantation. 1998; 7(3):319–326. [PubMed: 9647441]

Goldstein AS, Juarez TM, Helmke CD, Gustin MC, Mikos AG. Effect of convection on osteoblastic cell growth and function in biodegradable polymer foam scaffolds. Biomaterials. 2001; 22(11): 1279–1288. [PubMed: 11336300]

Grayson WL, Bhumiratana S, Cannizzaro C, Chao GP, Lennon D, Caplan AI, Vunjak-Novakovic G. Effects of initial seeding density and fluid perfusion rate on formation of tissue-engineered bone. Tissue Eng A. 2008; 14(11):1809–1820.

Grayson WL, Frohlich M, Yeager K, Bhumiratana S, Cannizarro C, Chan ME, Wan QL, Liu X, Guo XE, Vunjak Novakovic G. Engineering Anatomically-Shaped Human Bone Grafts. Proceedings of the National Academy of Sciences of the United States of America. 2009; 107(8):3299–3304. [PubMed: 19820164]

Grayson WL, Zhao F, Bunnell B, Ma T. Hypoxia enhances proliferation and tissue formation of human mesenchymal stem cells. Biochemical and Biophysical Research Communications. 2007; 358(3):948–953. [PubMed: 17521616]

Han YF, Cowin SC, Schaffler MB, Weinbaum S. Mechanotransduction and strain amplification in osteocyte cell processes. Proceedings of the National Academy of Sciences of the United States of America. 2004; 101(47):16689–16694. [PubMed: 15539460]

Hillsley MV, Frangos JA. Bone Tissue Engineering - The Role of Interstitial Fluid Flow. Biotechnology and Bioengineering. 1994; 43(7):573–581. [PubMed: 11540959]

Jacobs CR, Yellowley CE, Davis BR, Zhou Z, Cimbala JM, Donahue HJ. Differential effect of steady versus oscillating flow on bone cells. Journal of Biomechanics. 1998; 31(11):969–976. [PubMed: 9880053]

Liu XWS, Sajda P, Saha PK, Wehrli FW, Guo XE. Quantification of the roles of trabecular microarchitecture and trabecular type in determining the elastic modulus of human trabecular bone. Journal of Bone and Mineral Research. 2006; 21(10):1608–1617. [PubMed: 16995816]

Macpherson JV, Ohare D, Unwin PR, Winlove CP. Quantitative spatially resolved measurements of mass transfer through laryngeal cartilage. Biophysical Journal. 1997; 73(5):2771–2781. [PubMed: 9370471]

NIH-PA Author Manuscript

NIH-PA Author Manuscript

NIH-PA Author Manuscript

Maes F, Ransbeeck P, Van Oosterwyck H, Verdonck P. Modeling Fluid Flow Through Irregular Scaffolds for Perfusion Bioreactors. Biotechnology and Bioengineering. 2009; 103(3):621–630. [PubMed: 19288440]

Marolt D, Augst A, Freed LE, Vepari C, Fajardo R, Patel N, Gray M, Farley M, Kaplan D, Vunjak-Novakovic G. Bone and cartilage tissue constructs grown using human bone marrow stromal cells, silk scaffolds and rotating bioreactors. Biomaterials. 2006; 27(36):6138–6149. [PubMed: 16895736]

Martin I, Jakob M, Schafer D, Dick W, Spagnoli G, Heberer M. Quantitative analysis of gene expression in human articular cartilage from normal and osteoarthritic joints. Osteoarthritis and Cartilage. 2001; 9(2):112–118. [PubMed: 11237658]

Martin I, Smith T, Wendt D. Bioreactor-based roadmap for the translation of tissue engineering strategies into clinical products. Trends in Biotechnology. 2009; 27(9):495–502. [PubMed: 19651453]

Meinel L, Karageorgiou V, Fajardo R, Snyder B, Shinde-Patil V, Zichner L, Kaplan D, Langer R, Vunjak-Novakovic G. Bone tissue engineering using human mesenchymal stem cells: Effects of scaffold material and medium flow. Annals of Biomedical Engineering. 2004a; 32(1):112–122. [PubMed: 14964727]

Meinel L, Karageorgiou V, Hofmann S, Fajardo R, Snyder B, Li CM, Zichner L, Langer R, Vunjak-Novakovic G, Kaplan DL. Engineering bone-like tissue in vitro using human bone marrow stem cells and silk scaffolds. Journal of Biomedical Materials Research Part A. 2004b; 71A(1):25–34. [PubMed: 15316936]

Obradovic B, Meldon JH, Freed LE, Vunjak-Novakovic G. Glycosaminoglycan deposition in engineered cartilage: Experiments and mathematical model. Aiche Journal. 2000; 46(9):1860–1871.

Porter B, Zauel R, Stockman H, Guldberg R, Fyhrie D. 3-D computational modeling of media flow through scaffolds in a perfusion bioreactor. Journal of Biomechanics. 2005; 38(3):543–549. [PubMed: 15652553]

Radisic M, Deen W, Langer R, Vunjak-Novakovic G. Mathematical model of oxygen distribution in engineered cardiac tissue with parallel channel array perfused with culture medium containing oxygen carriers. American Journal of Physiology-Heart and Circulatory Physiology. 2005; 288(3):H1278–H1289. [PubMed: 15539422]

Radisic M, Malda J, Epping E, Geng W, Langer R, Vunjak-Novakovic G. Oxygen gradients correlate with cell density and cell viability in engineered cardiac tissue. Biotechnol Bioeng. 2006; 93(2): 332–43. [PubMed: 16270298]

Rossello RA, Wang Z, Kizana E, Krebsbach PH, Kohn DH. Connexin 43 as a signaling platform for increasing the volume and spatial distribution of regenerated tissue. Proceedings of the National Academy of Sciences of the United States of America. 2009; 106(32):13219–13224. [PubMed: 19628695]

Salvi JD, Lim JY, Donahue HJ. Finite Element Analyses of Fluid Flow Conditions in Cell Culture. Tissue Engineering Part C-Methods. 16(4):661–670. [PubMed: 19778171]

Sikavitsas VI, Bancroft GN, Holtorf HL, Jansen JA, Mikos AG. Mineralized matrix deposition by marrow stromal osteoblasts in 3D perfusion culture increases with increasing fluid shear forces. Proceedings of the National Academy of Sciences of the United States of America. 2003; 100(25): 14683–14688. [PubMed: 14657343]

Sikavitsas VI, Bancroft GN, Lemoine JJ, Liebschner MAK, Dauner M, Mikos AG. Flow perfusion enhances the calcified matrix deposition of marrow stromal cells in biodegradable nonwoven fiber mesh scaffolds. Annals of Biomedical Engineering. 2005; 33(1):63–70. [PubMed: 15709706]

Sikavitsas VI, Bancroft GN, Mikos AG. Formation of three-dimensional cell/polymer constructs for bone tissue engineering in a spinner flask and a rotating wall vessel bioreactor. Journal of Biomedical Materials Research. 2002; 62(1):136–148. [PubMed: 12124795]

Stains JP, Civitelli R. Cell-to-cell interactions in bone. Biochemical and Biophysical Research Communications. 2005; 328(3):721–727. [PubMed: 15694406]

NIH-PA Author Manuscript

NIH-PA Author Manuscript

NIH-PA Author Manuscript

Stiehler M, Bunger C, Baatrup A, Lind M, Kassem M, Mygind T. Effect of dynamic 3-D culture on proliferation, distribution, and osteogenic differentiation of human mesenchymal stem cells. Journal of Biomedical Materials Research Part A. 2009; 89A(1):96–107. [PubMed: 18431785]

Voronov R, VanGordon S, Sikavitsas VI, Papavassiliou DV. Computational modeling of flow-induced shear stresses within 3D salt-leached porous scaffolds imaged via micro-CT. Journal of Biomechanics. 43(7):1279–1286. [PubMed: 20185132]

Voronov RS, VanGordon SB, Sikavitsas VI, Papavassiliou DV. Distribution of flow-induced stresses in highly porous media. Applied Physics Letters. 97(2)

You J, Reilly GC, Zhen XC, Yellowley CE, Chen Q, Donahue HJ, Jacobs CR. Osteopontin gene regulation by oscillatory fluid flow via intracellular calcium mobilization and activation of mitogen-activated protein kinase in MC3T3-E1 osteoblasts. Journal of Biological Chemistry. 2001; 276(16):13365–13371. [PubMed: 11278573]

Yu XJ, Botchwey EA, Levine EM, Pollack SR, Laurencin CT. Bioreactor-based bone tissue engineering: The influence of dynamic flow on osteoblast phenotypic expression and matrix mineralization. Proceedings of the National Academy of Sciences of the United States of America. 2004; 101(31):11203–11208. [PubMed: 15277663]

Zeng Y, Cowin SC, Weinbaum S. A Fiber-Matrix Model for Fluid-Flow and Streaming Potentials in the Canaliculi of an Osteon. Annals of Biomedical Engineering. 1994; 22(3):280–292. [PubMed: 7978549]

Zhang D, Weinbaum S, Cowin SC. Electrical signal transmission in a bone cell network: The influence of a discrete gap junction. Annals of Biomedical Engineering. 1998; 26(4):644–659. [PubMed: 9662156]

Zhang W, Green C, Stott NS. Bone morphogenetic protein-2 modulation of chondrogenic differentiation in vitro involves gap junction-mediated intercellular communication. Journal of Cellular Physiology. 2002; 193(2):233–243. [PubMed: 12385001]

NIH-PA Author Manuscript

NIH-PA Author Manuscript

NIH-PA Author Manuscript

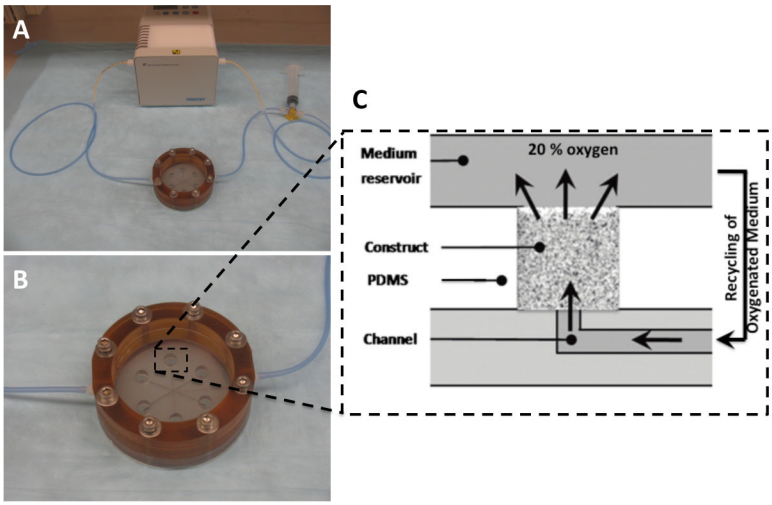

Figure 1. Bioreactor System

(**A**) Complete system including connector tubing and pump. (**B**) Close up of the bioreactor chamber (**C**) Schematic of circulating medium flow through a channel into a single construct and into the reservoir.

NIH-PA Author Manuscript

NIH-PA Author Manuscript

NIH-PA Author Manuscript

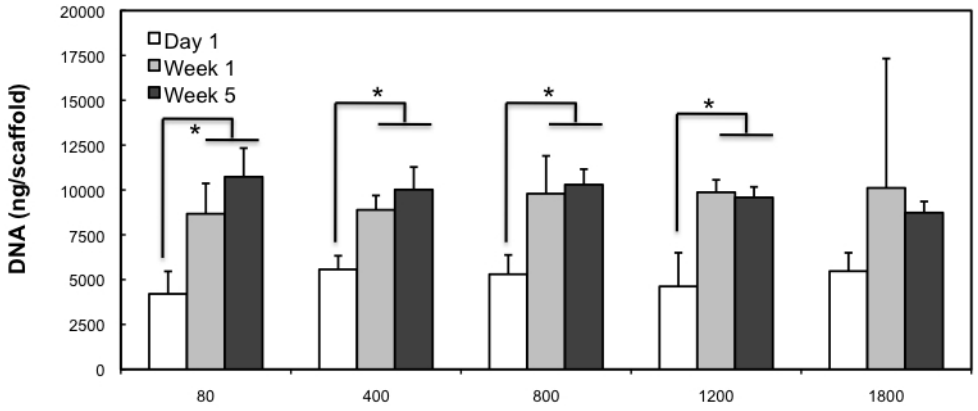

Figure 2. DNA content of engineered constructs

Total DNA per construct is shown for all experimental groups, at 1 day, 1 week and 5 weeks of cultivation. (*) denotes statistically significant differences between the groups ($n = 4$; $p < 0.05$).

NIH-PA Author Manuscript
NIH-PA Author Manuscript
NIH-PA Author Manuscript

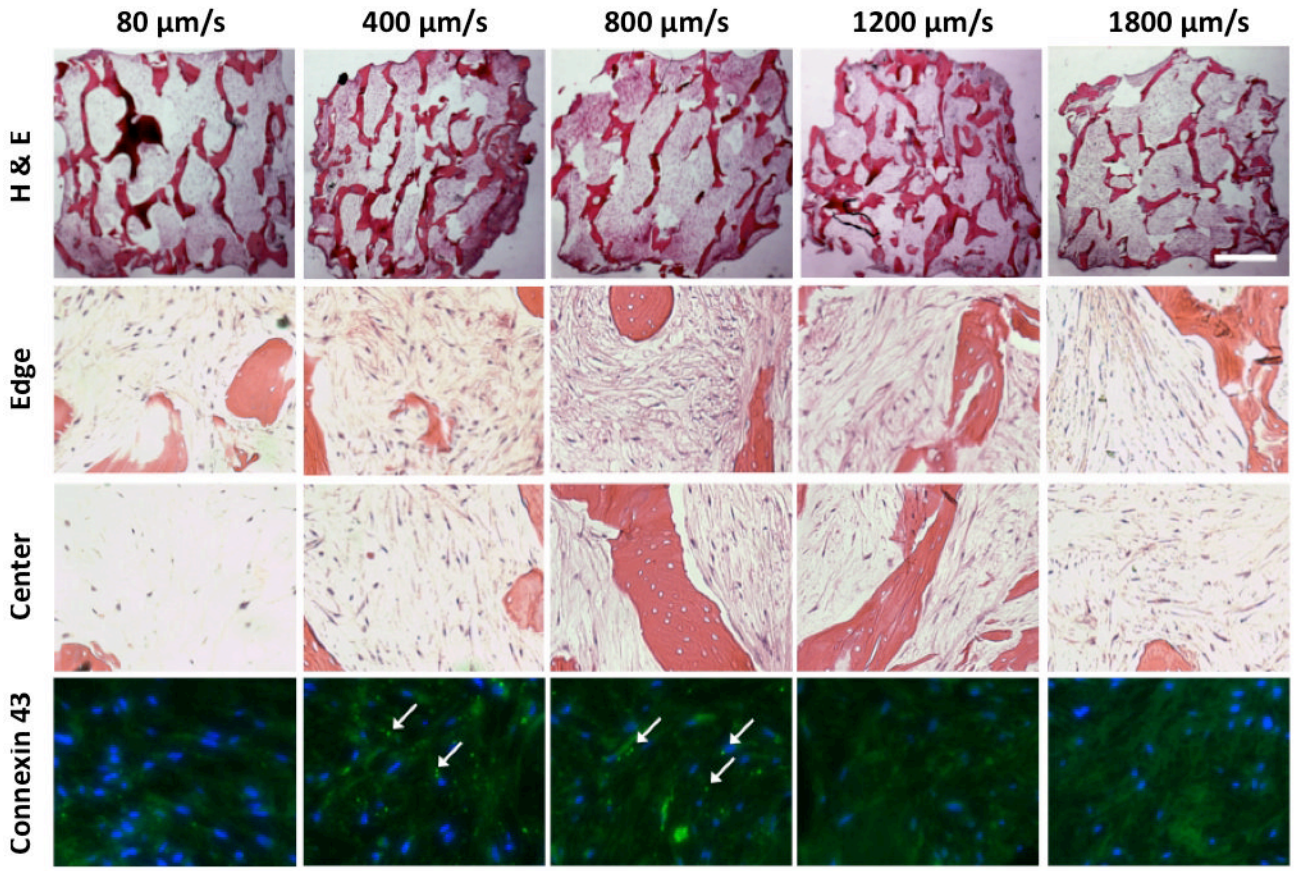

Figure 3. Histological assessment of engineered constructs

(**Top row**): H&E stains show cell and matrix distribution throughout the constructs Scale bar = 1 mm. (**Second row**): High magnification image of cell morphology at the construct edge. (**Third row**) Scale bars = 250 µm: Cell morphology at the construct center. (**Bottom row**): Connexin 43 expression (white arrows). Scale bar = 250 µm)

NIH-PA Author Manuscript

NIH-PA Author Manuscript

NIH-PA Author Manuscript

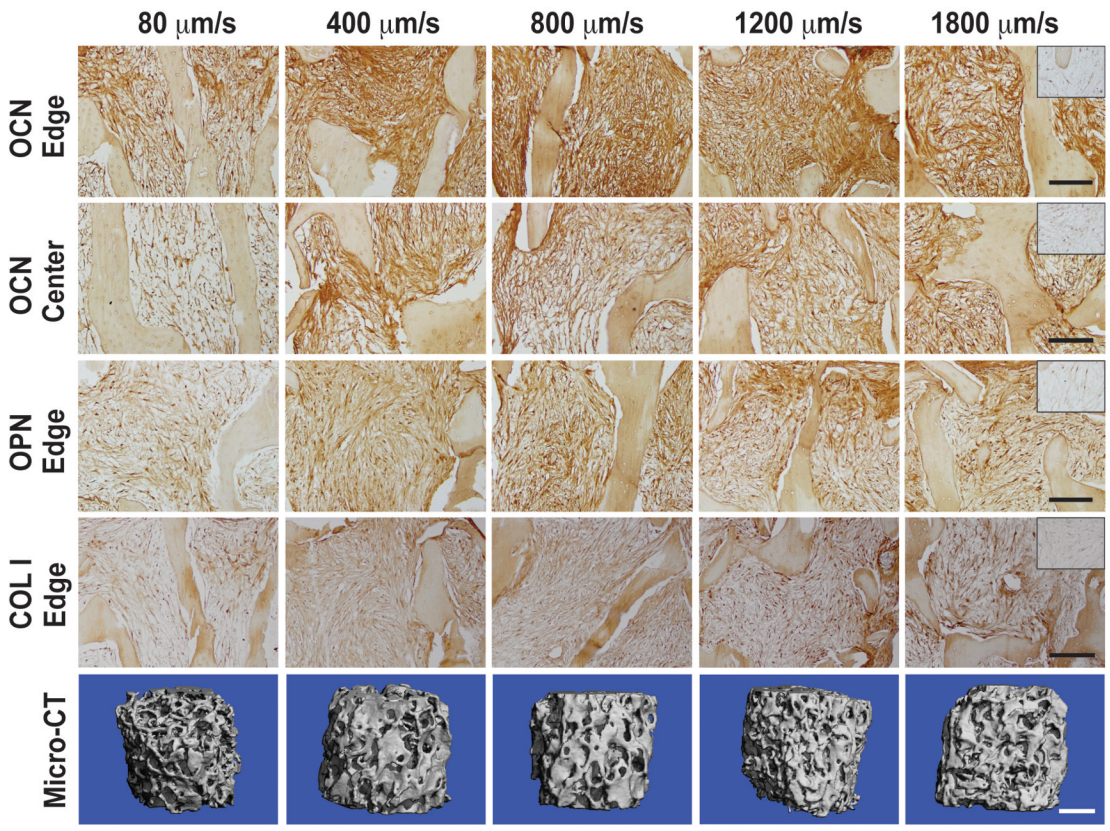

Figure 4. Accumulation of bone proteins and mineralized matrix

(**Top row**): Osteopontin (by immunostain). (**Second row**): Osteocalcin (by immunostain). (**Third row**): Collagen I (by immunostain). (**Bottom row**) (Scale bars = 1 mm): Mineralized matrix (by CT). Scale bar = 1 mm

NIH-PA Author Manuscript

NIH-PA Author Manuscript

NIH-PA Author Manuscript

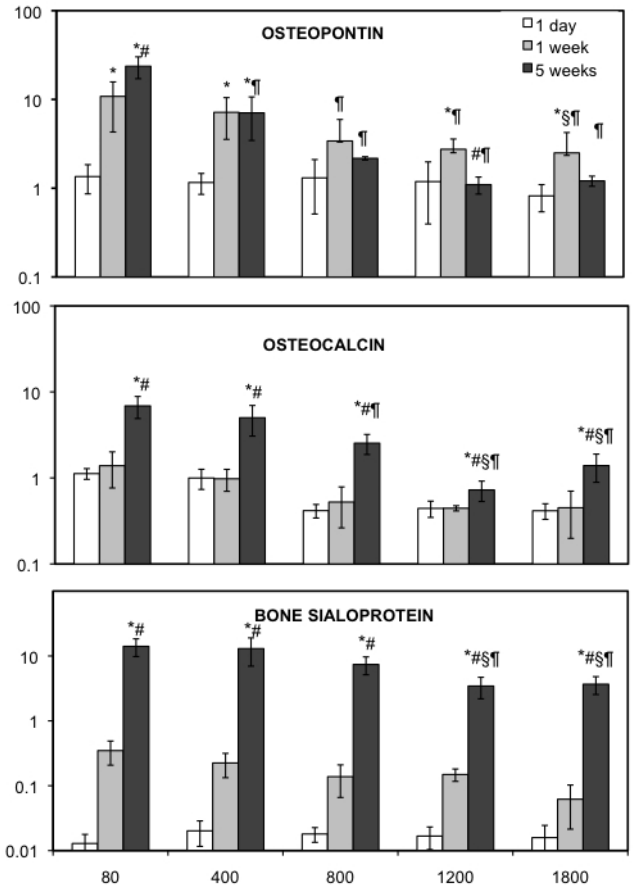

Figure 5. Gene expression

RT-PCR analysis of osteopontin, osteocalcin and bone sialoprotein gene expression at different time points. (n = 4; $p < 0.05$: * statistically different from day 1 value in the same group; # statistically different from week 1 in the same group; ¶ statistically different from 80 μm/s group at the same time point; § statistically different from 400 μm/s group at the same time point.)

NIH-PA Author Manuscript

NIH-PA Author Manuscript

NIH-PA Author Manuscript

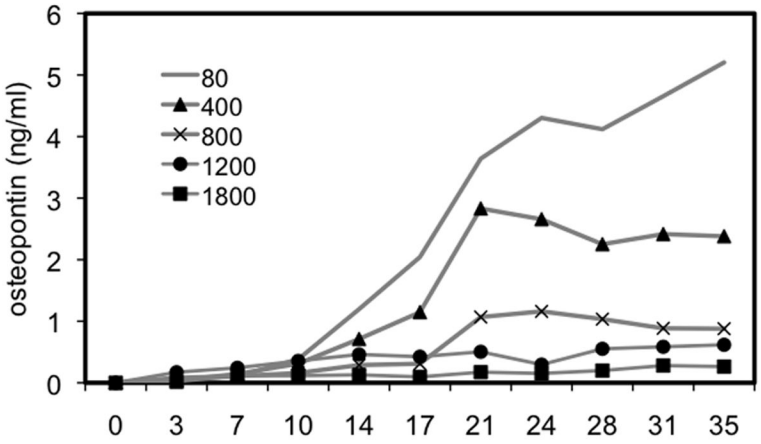

Figure 6. Osteopontin secretion into the medium

Data shown are the concentrations of osteopontin in culture medium at different time points, detected by ELISA.

NIH-PA Author Manuscript

NIH-PA Author Manuscript

NIH-PA Author Manuscript

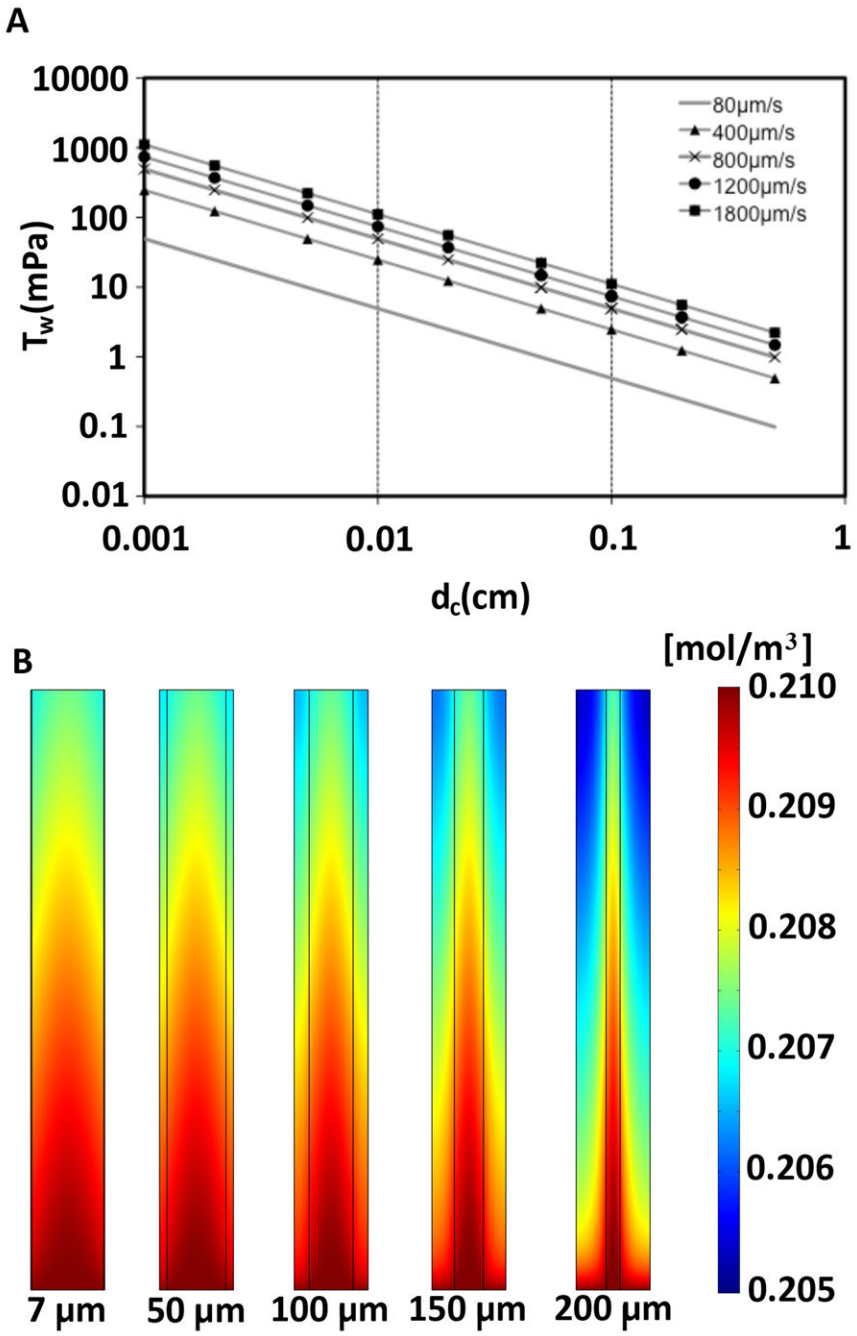

Figure 7. Model predictions for hydrodynamic shear stress and oxygen levels in engineered constructs

(**A**) The relationship between shear stress and channel diameter is shown for the various flow rates. The shaded region corresponds to the range of pore sizes present within the constructs. (**B**) The oxygen distribution in a single (500 μm diameter) channel is shown for cell layers of different thicknesses (7 μm – 200 μm) at the lowest flow rate (80 μm/s).